ACS APPLIED MATERIALS & INTERFACES

Research Article

www.acsami.org

Flexible and Transparent Polyimide Films Containing Two-Dimensional Alumina Nanosheets Templated by Graphene Oxide for Improved Barrier Property

I-Hsiang Tseng,*[,†] Mei-Hui Tsai,[‡] and Chi-Wei Chung[‡]

[†]Department of Chemical Engineering, Feng Chia University, No. 100, Wenhwa Road, Seatwen District, Taichung 40724, Taiwan

[‡]Department of Chemical and Materials Engineering, National Chin-Yi University of Technology, No. 57, Sec. 2, Chungshan Road, Taipin District, Taichung 41170, Taiwan

ABSTRACT: Unique two-dimensional alumina nanosheets (Alns) using graphene oxide (GO) as templates are fabricated and successfully incorporated with organo-soluble polyimide (PI) to obtain highly transparent PI nanocomposite films with improved moisture barrier property. The effects of filler types and contents on water vapor transmission rate (WVTR) and transparency of PI are systematically studied. The hydroxyl groups on GO react with aluminum isopropoxide via sol–gel process to obtain alumina coverd-GO (Al-GO), and then thermal decomposition is applied to obtain Alns. Alns are the most efficient fillers among others to restrict the diffusion of water vapor within PI matrix and simultaneously maintain the transparency of PI. XRD pattern, TEM, and AFM images confirm the sheet-like morphology of Alns with ultrahigh aspect ratio. With only 0.01 wt % of Alns, the PI nanocomposite film exhibits the most significant reduction of 95% in WVTR as compared to that of pure PI film. Most importantly, the resultant PI/Alns-0.01 film exhibits excellent optical transparency and high mechanical strength and great thermal stability.

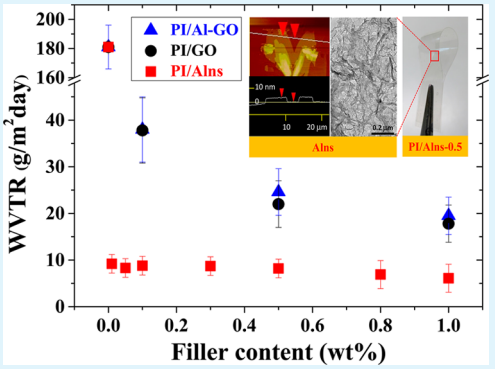

KEYWORDS: *graphene oxide, alumina, transparent polyimide, barrier, water-vapor-transmission-rate (WVTR)*

1. INTRODUCTION

Colorless polyimide (PI) films are promising flexible substrates for advanced electronic applications because of their excellent optical, mechanical, and thermal properties.[1,2] However, the barrier performance of polymers critically affects the reliability of those devices using polymers as substrates.[3−5] Several approaches have been developed to reduce the water/gas permeation rate through polymeric films.[3−17] Nanofillers, such as alumina, silica, clay, and graphene, have been selected to incorporate within the polymer matrix or to deposit on the surface of polymer to extend the gas pathway through the polymer film. For example, the permeation of water in polyamide containing less than 2.5 vol % of montmorillonite can be described by the tortuous model.[17] In addition, the presence of sheet-like nanoparticles in polymer matrix could affect the crystallinity degree of polymer and thus govern the permeability of water or gas in polymer.[3,8,17,18] Our previous studies demonstrate the significant reduction in water vapor transmission rate (WVTR) of PI films by blending small amounts of graphene oxide (GO) or reduced graphene oxide (RG) nanosheets.[6,16] With the loading of 0.1 wt % RG, the WVTR can be reduced to 13 g/m^2·day, as compared to 31 g/m^2·day for PI film containing the same amount of GO. In addition, it has been observed that the barrier property of alumina by atomic layer deposition on Kapton is superior to that of silica.[12] In an earlier study,[11] we also prepared traditional aromatic PI films containing up to 15 wt % of alumina by in situ polymerization. However, the WVTR of these PI/Al_2O_3 increases with increasing Al_2O_3 contents. The spherical alumina particles with the diameter of 90 nm in these PI films are not good gas diffusion barrier materials but excellent anchors for PI chains during thermal treatment.

Hence, the two-dimensional and ultrathin nanofillers are promising fillers for PI films to exhibit improved water barrier property and maintain excellent optical transparency. Suchanek et al. synthesized α-alumina via a hydrothermal process.[18] They controlled the morphology of alumina by tuning the type and concentration of the modifier. The obtained α-alumina nanosheets have the aspect ratio ranging from 7 to 200 and the thicknesses between 10 and 75 nm. However, the reaction condition requires high temperature and pressure (400 °C and 10 MPa) and long reaction time (more than 6 days). A relatively feasible sol–gel process has been developed to synthesize Al(OH)$_3$-functionalized graphene.[19] The hydroxyl groups on GO will form hydrogen bonding to the alumina hydroxide hydrolyzed from aluminum isopropoxide (AlIP). Hence, we utilize the same principle to cover the surface of GO with alumina hydroxide, followed by the thermal decom-

Received: May 14, 2014
Accepted: July 7, 2014
Published: July 16, 2014

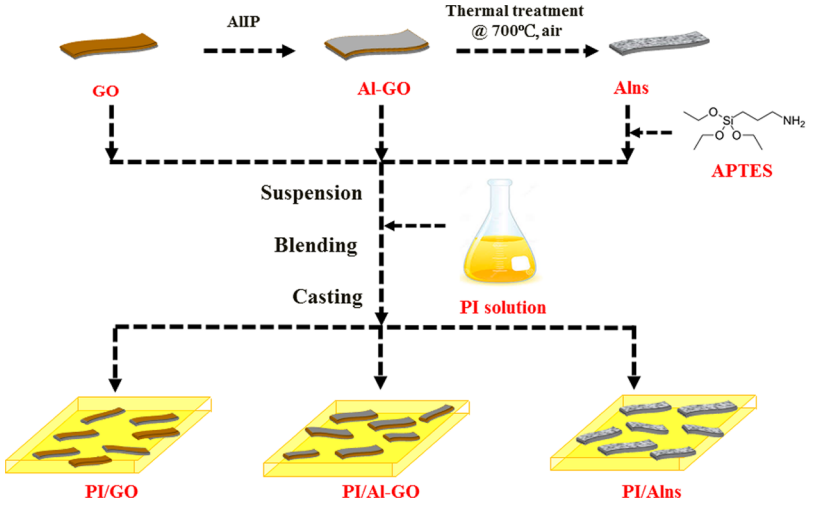

Figure 1. Schematic procedure to prepare fillers and PI nanocomposite films.

position of GO templates. The residuals of alumina nanosheets (Alns) with ultrahigh aspect ratio and silk-like morphology are the candidate fillers for transparent PI. The barrier performance of transparent PI films containing Alns is investigated as well as the effects of Alns contents on the optical, thermal, and mechanical properties. The characteristics of fillers are explored, and the dispersion of fillers in PI is compared. Notably, we have discovered that the Alns are perfect fillers to restrain moisture permeation and simultaneously maintain visible light transportation within transparent PI matrix. To the best of our knowledge, this is the first report about the improvement of barrier property of transparent PI by two-dimensional alumina nanosheets using GO as templates.

2. EXPERIMENTAL SECTION

2.1. Materials. Bicyclo[2.2.2]oct-7-ene-2,3,5,6-tetracarboxylic dianhydride (BCDA) and 3,4′-oxidianiline (3,4′-ODA) from Aldrich were used as-received. Cosolvents γ-butyrolactone (GBL) from ECHO and dimethylacetamide (DMAc) from TEDIA were dried overnight with molecular sieves before use. Methanol and ethanol from ECHO were used as received. The catalyst isoquinoline, HCl, H_2SO_4, H_2O_2, $KMnO_4$, and aluminum isopropoxide (AlIP) were commercially obtained from TCI. The coupling agent (3-aminopropyl) triethoxysilane (APTES) was purchased from Acros. Graphite powder (325 mesh) was supplied by Alfa-Aesar.

2.2. Synthesis of Plate-Like Fillers. A modified Hummers method was utilized to synthesize GO powder from graphite.[16,20] AlIP was dispersed in methanol−water mixture at 90 °C for 30 min to process the hydrolysis process[19] and followed by the mixing of GO at 60 °C for 1 day. The molar ratio of AlIP to GO was adjusted to obtain fillers with various coverage degrees on GO. The alumina-grafted GO (Al-GO) nanosheets were obtained after the filtration and vacuum-dried at 70 °C. The sample code of Al-GO filler is Al-GO (*x*:*y*), where *x* and *y* are the relative molar ratio of Al to GO. The obtained Al-GO was further thermal treated from room temperature to 600−700 °C for 10 min to obtain Alns. The sample code of Alns is denoted Alns-*z*, where *z* represents the temperature of thermal treatment.

2.3. Synthesis of PI Nanocomposite Films. Organo-soluble PI with solid content of 20 wt % was synthesized from the reaction of equal molar BCDA and 3,4′-ODA in cosolvent via one-step method.[21] To maintain the optical transparency of PI, isoquinoline (2 wt % of PI solid content) was employed to complete the chemical imidization process rather than the thermal imidization. The homogeneous solution was refluxed at 170 °C for 16 h to complete the imidization process. The resultant viscous and transparent PI solution was slowly decanted into excess methanol to solidify PI. The PI precipitate was washed by continuously stirring in methanol to remove unreacted monomers or a fraction of low molecular weights. After being dried in a vacuum oven at 150 °C, the collected PI precipitate can be stored or easily redissolved in DMAc for further casting or blending procedure. The dried PI precipitate (1.5 g) was completely dissolved in DMAc to obtain PI solution with the solid content of 20 wt % at ambient condition. For preparing PI containing 0.1 wt % of fillers, 0.0015 g of fillers (GO, Al-GO (3:3), or Alns-700) was dispersed in DMAc with the assistance of ultrasonication for 2 h and then mixed with the above PI solution as illustrated in Figure 1. The degassed solution was cast on a clean glass substrate by a doctor-blade with the gap of 250 μm. The curing temperature was increased at a rate of 20 °C/h from 80 to 100, 140, 160, 180, 190, and 200 °C, isothermal holding for 1 h at each temperature, and finally to 210 °C for 5 h. The sample code was denoted PI/GO-*w*, PI/Al-GO-*w*, or PI/Alns-*w*, where *w* is the wt % of fillers in PI matrix. For synthesizing PI/Alns nanocomposite films, coupling agent APTES (20 wt % of Alns) was added to the PI/Alns solution to improve the compatibility between two phases.

2.4. Characterization of PI Nanocomposites. X-ray diffraction (XRD) experiments were conducted on an X-ray diffractometer (PANalytical X'Pert PRO) using Cu Kα radiation (λ = 0.154 nm) at an accelerating voltage of 40 kV and current of 30 mA to study the crystalline structure of nanofillers used in this study. An X-ray photoelectron spectrometer (XPS) (ESCA PHI-1600, Physical Electronics) was used to compare the surface composition of fillers. The field emission scanning electron microscope (FE-SEM, JEOL JSM-7401F) was performed at an acceleration voltage of 15 kV to observe the morphology of fillers and films. The fractured surface of each PI nanocomposite film was obtained by fracturing the frozen films upon the immersion in liquid nitrogen. The transmission electron microscope (TEM, JEOL JEM-2100F) equipped with EDS (OXFORD, X-MAX) was also applied at an acceleration voltage of 200 kV to observe the morphology of fillers and the dispersion of fillers in PI. The thickness of Alns was identified by an atomic force microscope (AFM, VEECO, Dimension 5000) with the scan rate of 1 Hz and the scan area of 40 μm. The dilute Alns dispersion was drop-cast on a precleaned silicon wafer. Infrared spectra of PI were recorded by using a Nicolet Protégé-460 Fourier transform infrared (FTIR) spectrophotometer equipped with a variable-temperature sample holder. The optical transmittance of each film spin-coated on the optical glass was examined by a UV−vis spectrophotometer (HUNTERLAB, Ultrascan VIS). The water vapor transmission rate (WVTR) of each sample with the size of 10 cm^2 was measured using a permeation test system (MOCON, Permatran-W 3/61) at atmospheric pressure, 40 °C, and 100% relative humidity (RH). The WVTR (g/m^2·day) of each sample multiplied by film thickness is the water vapor permeation with the unit of g·mil/m^2·day. In this study, the thickness of each synthesized film is around 25 μm, which is equal to

the commercially used thickness unit 1 mil. The thickness of each film is listed in Table 1. The dynamic mechanical analysis (DMA) was performed with a Dupont DMA-2980 at a frequency of 1 Hz, from 60 to 350 °C, and at a heating rate of 3 °C/min. Thermogravimetric analysis (TGA) was carried out with a TGA-Q500 from TA Instrument at a heating rate of 20 °C/min under nitrogen for PI films and under air for fillers, respectively. The thermal mechanical analyzer (TMA, TA Instrument, Q-400) was conducted under an extension mode, with a tension force of 0.05 N, at a heating rate of 10 °C/min, at a frequency of 1 Hz, and under nitrogen. The coefficient of thermal expansion (CTE) was determined by the dimension change in the temperature range of 100−200 °C, which is the commonly applied testing condition in manufactures. Water absorption is used to determine the amount of water absorbed of each film under ambient conditions. Fixed amounts of specimens are dried in a vacuum oven at 80 °C for 24 h and then cooled to 25 °C. Immediately upon cooling the specimens are weighed. Each sample is then submerged in water at 25 °C for 24 h. After being removed from the water bath, each sample is patted dry and weighed. Water absorption of each film is expressed as increase in weight percent.

Table 1. Thickness, Mechanical, and Thermal Properties of Pure PI and PI Nanocomposite Films

film	thickness (μm)	T_g[a] (°C)	T_d^5[b] (°C)	CTE[c] (ppm/°C)	TS[d] (MPa)	E'[e] (MPa)
PI	25	349	420	54	58	1487
PI/Alns-0.1	29	348	421	52	60	1984
PI/Alns-0.3	27	353	436	48	63	2106
PI/Alns-0.5	27	353	440	50	68	2247
PI/Alns-0.8	24	351	430	41	70	2300
PI/Alns-1.0	30	352	419	50	70	2606
PI/Al-GO-1.0	28	350	419	33	73	2616
PI/GO-1.0	28	347	436	42	76	2471

[a]The temperature at the maximum of tan δ curve is designated as T_g. [b]The thermal decomposition temperature at 5% weight loss is designated as T_d^5. [c]The coefficient of thermal expansion (CTE) is determined over the range of 100−200 °C. [d]The tensile strength (TS) is the maximum stress before break. [e]The storage modulus (E') at 60 °C.

3. RESULTS AND DISCUSSION

3.1. Characteristics of Fillers. To optimize the coverage of alumina hydroxide on GO, various amounts of AlIP are initially applied to the sol−gel process. The thermogravimetric curves of obtained Al-GO with various ratios of AlIP to GO are shown in Figure 2. It is similar to the TGA curve of GO; the loosely bounded water molecules on all Al-GO are eliminated upon the temperature increases from room temperature to around 160 °C. The effect of AlIP to GO ratio on this weight loss is negligible. The first weight loss percentage (15%) of each Al-GO is greater than that (10%) of GO, indicating more water molecules adsorbing on Al-GO.[22] There is no difference between the amounts of adsorbed water on Al-GO fillers. The following weight loss stage starting at 200 °C for all Al-GO and GO is the result of the decomposition of epoxy or carboxyl groups on GO.[22,23] The weight loss percentage of around 35% is achieved for all Al-GO and GO fillers heated to 250 °C, suggesting a similar content of those labile oxygen groups on GO structure. The final thermal decomposition of GO or Al-GO starting at 500 °C and leveling off at 600 °C is related to the removal of basal plane oxygen-containing groups, such as phenolic hydroxyl groups. The phenolic form hydroxyl groups have been found the most stable functional groups on GO.[22] The final decomposition stage of Al-GO is not as rapid as GO because some of the hydroxyl groups on GO have been consumed during the sol−gel process. Hence, the higher is the content of AlIP in Al-GO, the fewer are the hydroxyl groups on GO. The obtained Al-GO (3:3) has the char yield of 20% at 700 °C as compared to 13% for Al-GO (1:3). The char yield of GO at 600 °C is 10%. Because Al-GO (3:3) has relatively high alumina content as proved by the following SEM/EDS results, it is selected as the precursor of Alns. The thermal treatment temperature ranging from 600 to 700 °C was performed on Al-GO (3:3). Figure 2 also displays the linear TGA curve of Alns-700, which was obtained from Al-GO (3:3) after being thermally treated at 700 °C. The thermal stability of Alns-700 is high that only a 5% decrease in weight is observed at 750 °C.

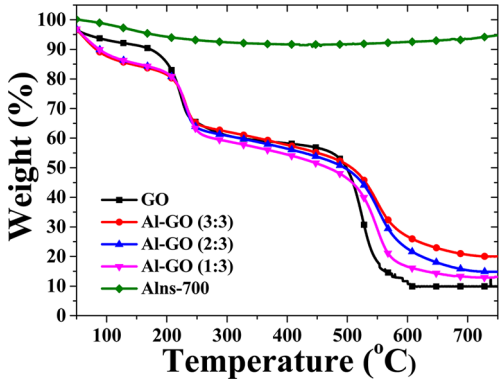

Figure 2. Thermogravimetric curves of GO, Al-GO, and Alns.

The SEM images and the corresponding EDS analysis shown in Figure 3a−c display the morphology and the composition differences between Al-GO fillers containing various amounts of alumina. In addition to the stacks of GO sheets, the surface of GO is covered with alumina. The coverage of alumina increases with increasing AlIP content as evidenced by the EDS of each image. The detected atomic ratio of aluminum as summarized in Table 2 is 0.89% for Al-GO (1:3) and increases to 1.46 for Al-GO (3:3). When thermal treatment was applied to the filler Al-GO (3:3), the obtained Alns displays a significant increase in both aluminum and oxygen content. The aluminum and oxygen ratio for Alns-700 is 12.74% and 56.38%, respectively, as compared to 10.55% and 51.00% for Alns-600. Figure 3d−f exhibits the morphology of those Alns fillers obtained from different temperatures. Instead of the sphere alumina particles, the stacked lamellar structure is observed from Alns thermal-treated at various temperatures. The thermal treatment increases the content of alumina on Alns. In addition to the highest alumina content, the Alns shown in Figure 3f has the thinnest structure, suggesting the best candidate as the filler for transparent PI with improved barrier properties. Alns-700 with sheet-like and ultrathin features adopted from GO are perfectly displayed from the TEM images of Figure 4. In contrast to the smooth surface of GO, more wrinkles or folded regions are observed from Alns-700. The recorded atomic ratio of Alns-700 from the TEM image is 26.25% for Al and 54.00% for O. The carbon content of Alns-700 reduces to less than 20%, as compared to 85.10% for GO. The AFM image and the corresponding height scan of the indicated line present that the thickness of Alns is around 4.2 nm as shown in Figure 4c. Combined with the longer edge length of Alns, which is at least 5 μm as observed in TEM or AFM images, the aspect ratio of Alns is higher than 1000.

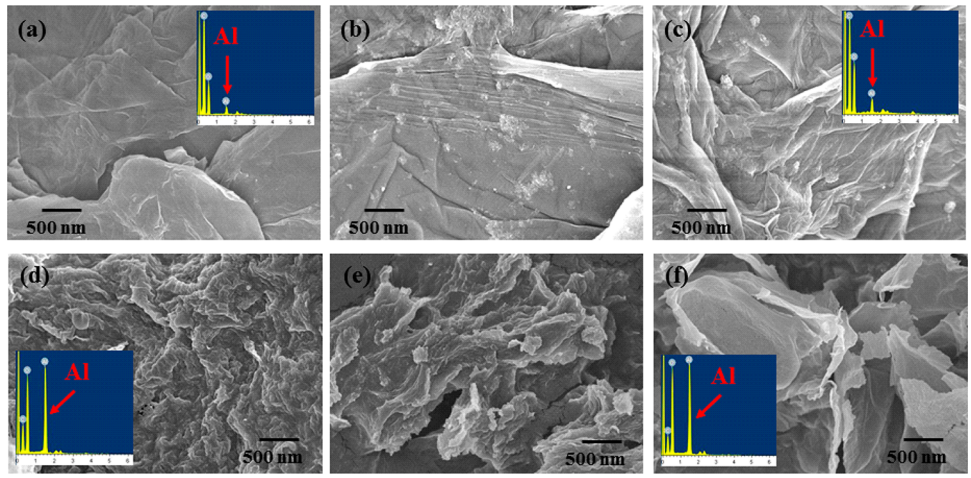

Figure 3. SEM images of (a) Al-GO (1:3), (b) Al-GO (2:3), (c) Al-GO (3:3), (d) Alns-600, (e) Alns-650, and (f) Alns-700. Insets: EDS results of the corresponding images.

Table 2. Atomic Ratio of Each Filler Determined from the EDS Results of the Corresponding SEM Images

	atomic ratio (%)			
filler	C	O	Al	EDS results from Figure
GO	85.10	14.90		4a
Al-GO (1:3)	66.04	33.07	0.89	3a
Al-GO (3:3)	59.20	39.34	1.46	3c
Alns-600	38.45	51.00	10.55	3d
Alns-700	30.88	56.38	12.74	3f
	19.75	54.00	26.25	4b

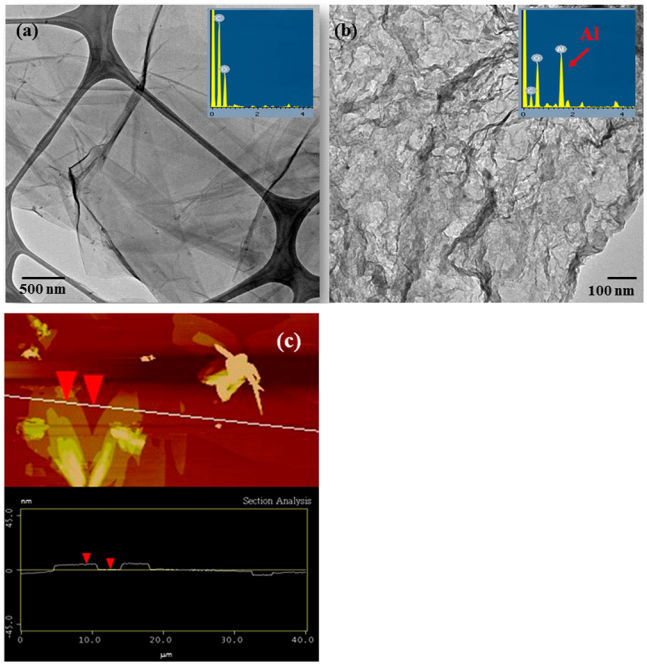

Figure 4. TEM images of (a) GO and (b) Alns-700. Insets: EDS results of the corresponding images. (c) AFM image and the height scan of the indicated line of Alns-700.

Those results suggest that the two-dimensional Alns are successfully prepared via the sol–gel process of AlIP on GO and the following thermal treatment at 700 °C.

The crystalline structure of each filler is determined by the XRD patterns shown in Figure 5. The disappearance of the

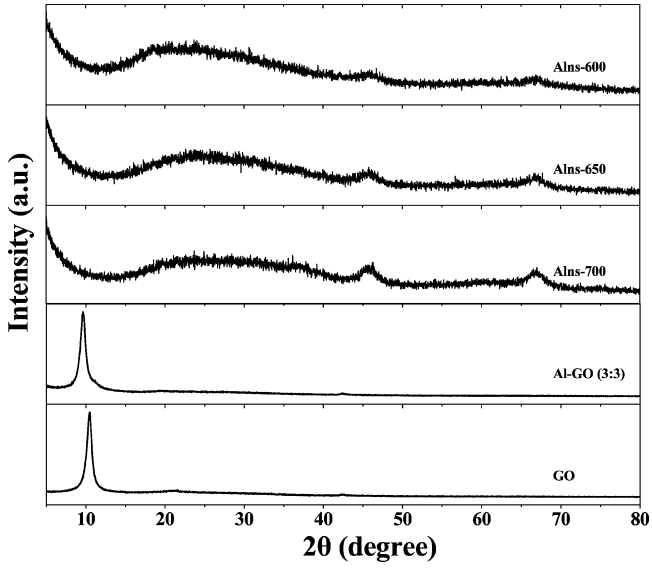

Figure 5. XRD patterns of GO, Al-GO, and Alns fillers.

characteristic graphite peak at 26.4° (d = 0.34 nm) and the formation of a diffraction peak at 2θ of 10.5° (d = 0.84 nm) from GO indicate the successful exfoliation by intercalation of oxygen-functional groups in the graphite interlayer.[24] A continuous intercalation is achieved via the sol–gel process of AlIP on GO that Al-GO (3:3) exhibits a characteristic diffraction peak at 9.6° (d = 0.92 nm). The following annealing process on Al-GO (3:3) at different temperatures not only removed most of the GO but slightly affected the crystalline structure of alumina. The broad diffraction peaks ranged from the 2θ of 15° to 30°, indicating amorphous structure of Alns. The intensity of peaks centered at 37.1°, 45.6°, and 66.8° slightly increases with the increasing annealing temperature. Those diffraction peaks of Alns fillers have neither AlOOH nor alumina obtained from the literature.[25−27] Those characteristic peaks are believed to be a mixture of doyleite and nordstrandite aluminum trihydroxide structure on the surface of GO.[28]

dx.doi.org/10.1021/am502962b | ACS Appl. Mater. Interfaces 2014, 6, 13098−13105

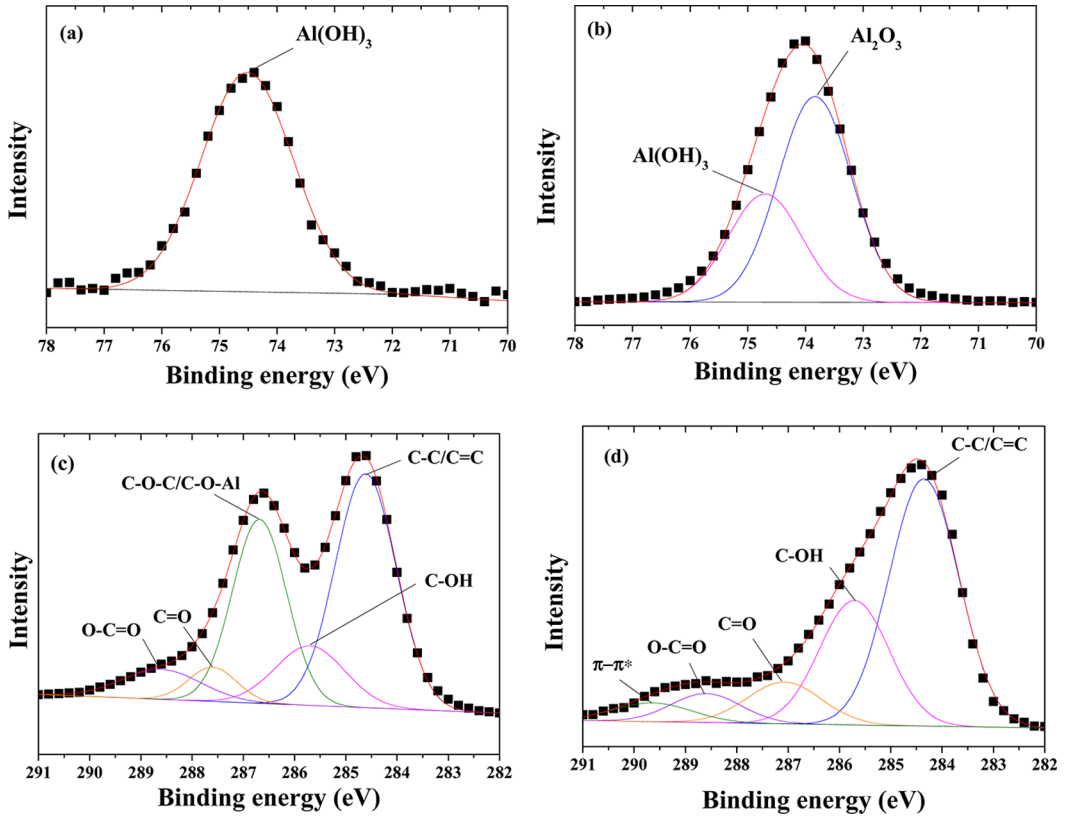

Figure 6. XPS Al 2p spectra of (a) Al-GO (3:3) and (b) Alns-700. XPS C 1s spectra of (c) Al-GO (3:3) and (d) Alns-700.

The XPS spectra shown in Figure 6 are applied to identify the surface chemical structure of fillers, and Table 3 summarizes

Table 3. Surface Atomic Ratio of Each Filler Determined from the XPS Analysis

	atomic ratio (%)		
filler	C	O	Al
GO	70.0	30.0	
Al-GO (3:3)	70.0	29.0	1.0
Alns-700	19.0	61.0	20.0

the surface atomic ratio of fillers. The oxygen concentration for GO is 30% as compared to 29% for Al-GO (3:3). Only 1% of aluminum is detected from the surface of Al-GO (3:3). For Alns-700, the aluminum and oxygen concentration increases to 20% and 61%, respectively. A significant decrease in carbon content confirms the removal of abundant carbon species during the thermal treatment at 700 °C. The surface composition of Alns-700 detected by XPS is consistent with the results detected from TEM/EDS, suggesting the ultrathin feature of Alns. Figure 6a and b shows the Al 2p core level spectra for Al-GO and Alns, respectively. For Al-GO, the main peak with the binding energy of 74.5 eV is assigned to $Al(OH)_3$. The additional deconvoluted peak centered at 73.8 eV for Al-GO comes from the Al_2O_3 species.[19,29] The assignments of C 1s components on Al-GO are sp^2 and sp^3 graphite at 284.5 eV and other oxygen functional groups at higher binding energy. The typical oxygen functional groups on GO, including hydroxyl (285.5 eV), epoxy (286.5 eV), carbonyl (287.5 eV), and carboxyl groups (288.5 eV),[20,22,30] are observed from Figure 6c. After the annealing process on Al-GO, the obtained Alns reveals weaker C 1s signals, and the deconvoluted peaks are available in Figure 6d. The peak intensity of C−O−C or C−O−Al on Alns decreases after the thermal treatment. In addition to the graphitic C−C, C═C, and above-mentioned oxygen-containing groups, the weak $\pi-\pi^*$ shakeup peak centered at 289.8 eV is observed, indicating slightly increased aromaticity of residual GO within Alns.[23]

3.2. Characteristics of PI Nanocomposite Films. The barrier property of PI nanocomposites is evaluated by comparing the WVTR of each film with a fixed area of 10 cm^2 using a steady-state permeation test system. As shown in Figure 7, the WVTR of pure PI film is around 180 g/m^2·day and decreases with the increasing amounts of fillers in PI. The

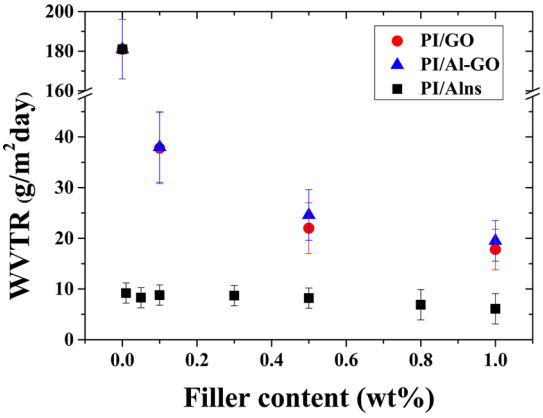

Figure 7. Effects of filler content and type on the WVTR of PI nanocomposites. Note: The filler in PI/Al-GO is Al-GO (3:3); the filler in PI/Alns is Alns-700.

dx.doi.org/10.1021/am502962b | ACS Appl. Mater. Interfaces 2014, 6, 13098−13105

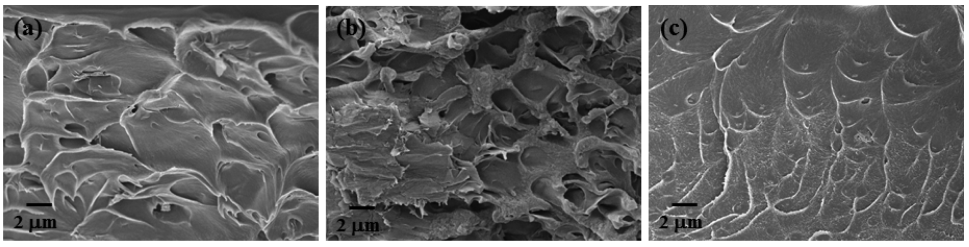

Figure 8. SEM images of the fracture surface of (a) PI/GO-1.0, (b) PI/Al-GO-1.0, and (c) PI/Alns-1.0 films. Note: The filler in PI/Alns-1 is Alns-700.

reduction trend in WVTR by blending 0.1−1.0 wt % of GO or Al-GO (3:3) in PI matrix is similar. The average WVTR for PI/GO-0.1 or PI/Al-GO-0.1 is all around 38 g/m^2·day. In contrast, blending the same amount of Alns-700 in PI leads to a significant drop in WVTR, which is around 9 g/m^2·day. When we keep reducing the content of Alns to the lowest feasible one, 0.01 wt %, the WVTRs of those PI/Alns leveled off to the value of 8−9 g/m^2·day. In other words, there is only 0.01 wt % of Alns-700 in PI matrix, and the resultant PI film has a 95% reduction in WVTR as compared to pure PI film.

It is believed that the uniform distribution of those high-aspect-ratio nanosheets by the assistance of coupling agent in PI matrix can effectively extend the path of the water vapor passing through the thin film[3,9,17,31] and thus significantly improve water vapor barrier property. To determine the dispersion of fillers in PI matrix, the fracture surface of each PI nanocomposite containing 1.0 wt % of fillers is examined by SEM images as shown in Figure 8. The wrinkled features of GO, Al-GO, and Alns can be easily distinguished from the PI matrix. Moreover, the plastic deformation from the fractured surfaces revealed the strong interactions between two phases especially in PI/Alns-1. In Figure 8c, a relatively dense fracture surface of PI/Alns-1 film suggests the excellent compatibility between Alns and PI with the assistance of tiny amounts of coupling agent. In contrast, some aggregation of Al-GO is observed from Figure 8b. The 24-h water absorption amount for PI/Alns-1 is 3.3%, which is lower than that of pure PI (7.3%) and both PI/GO-1 and PI/Al-GO-1 (6.8%), suggesting a denser PI matrix in PI/Alns-1 than in other films. In addition, the contact angles of PI/GO-0.5, PI/Al-GO-0.5, and PI/Alns-0.5 are 76°, 72°, and 71°, respectively, which are higher than that of pristine PI (64°). The presence of those fillers in PI provides the hydrophobic feature of PI and thus decreases the WVTR of composite films. Moreover, the well dispersion of Alns in PI increases the tortuosity of water transportion path,[17] which plays the key role in the reduction of water permeation. Alns-700 is the most suitable water barrier filler to well disperse in PI matrix and thus create a dense PI matrix to hinder water transportation and, most importantly, to retain the optical transparency of PI films.

The optical property of PI nanocomposite films spin-coated on optical glasses with the average thickness of 10 μm is evaluated by comparing their transmittance in visible light region. Figure 9 shows the UV−vis spectra of PI films containing various amounts of GO, Al-GO (3:3), and Alns-700. The optical transparency of PI nanocomposite films decreases with the content of filler, especially for Al-GO (3:3). For the same filler concentration of 1 wt %, the transmittance at 550 nm reduces to 85.0% for PI/Al-GO, and 89.3% for PI/GO, respectively. Surprisingly, the optical transmittance for PI/Alns-1 is as high as 96.3%, indicating the excellent transparency of

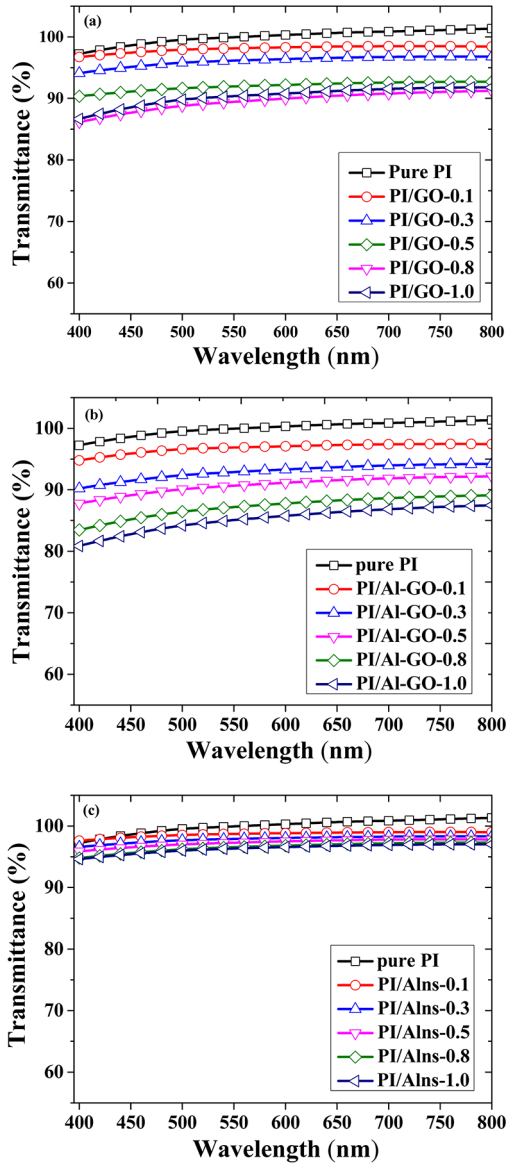

Figure 9. UV−vis spectra of (a) PI/GO, (b) PI/Al-GO, and (c) PI/Alns nanocomposite films with the average thickness of 10 μm in the visible light region. Note: The filler in PI/Al-GO is Al-GO (3:3); the filler in PI/Alns is Alns-700.

Alns and the well dispersion of Alns in PI matrix. When the Alns content decreases to 0.1 wt %, the optical transmittance of PI nanocomposite film is even higher at 98.5%. Recall that the PI/Alns-0.1 also exhibits excellent moisture barrier property among other PI nanocomposites containing GO or Al-GO.

dx.doi.org/10.1021/am502962b | ACS Appl. Mater. Interfaces 2014, 6, 13098−13105

The mechanical and thermal properties of PI nanocomposites films are summarized in Table 1. The glass transition temperature (T_g) of pure PI is 347 °C and slightly increases with the Alns contents in PI matrix. For PI/Alns-1.0, the T_g value is 352 °C. The variation in T_g values with Al-GO or GO content is negligible. The T_g value is 350 °C for PI/Al-GO-1.0 and 347 °C for PI/GO-1.0, respectively. The thermal decomposition temperature (T_d^5) at 5% weight loss of PI/Alns is 1−10 °C higher than that of pure PI (420 °C), suggesting the sufficient thermal stability for industry application. In addition, high dimensional stability is essential for PI-based nanocomposites as they are commonly laminated with copper, and followed by high temperature process. The coefficients of thermal expansion (CTEs) of PI/Alns nanocomposites ranging from 40 to 52 ppm/°C are lower than that of pure PI (54 ppm/°C). The incorporation of 1.0 wt % of Al-GO in PI matrix significantly decreases the CTE to 33 ppm/°C as compared to 42 ppm/°C for PI/GO-1.0 and 50 ppm/°C for pure PI/Alns-1.0, respectively. The addition of two-dimensional Al-GO in PI matrix may effectively restricts the segmental mobility of PI, and thus a lower CTE is observed as compared to other two fillers.[32] Both the tensile strength (TS) and the storage modulus of PI/Alns increase with the Alns contents, indicating well dispersion of Alns, and sufficient interaction between PI matrix and fillers.[33]

4. CONCLUSION

By using GO as templates, ultrathin and two-dimensional Alns are successfully obtained and served as the excellent filler for transparent PI. Only by blending 0.01 wt % of Alns in PI did the PI/Alns-0.01 nanocomposite film show improved barrier property and, most importantly, maintain superior optical transparency, sufficient mechanical strength, and high thermal stability. The transparent, flexible, and electrically insulating PI nanocomposites are promising substrate materials for electronic applications.

AUTHOR INFORMATION

Corresponding Author

*Tel.: +886 4 24517250 ext. 3666. Fax: +886 4 24510890. E-mail: ihtseng@fcu.edu.tw.

Notes

The authors declare no competing financial interest.

ACKNOWLEDGMENTS

We would like to acknowledge financial support from the Ministry of Science and Technology of Taiwan under grant numbers NSC102-2221-E-167-034-MY2 and NSC102-2218-E-035-005-MY2. We also appreciate the Precision Instrument Support Center of Feng Chia University for providing AFM and TGA measurement facilities.

REFERENCES

(1) Liu, J. M.; Lee, T. M.; Wen, C. H.; Leu, C. M. High-Performance Organic-Inorganic Hybrid Plastic Substrate for Flexible Displays and Electronics. *J. Soc. Inf. Dispersion* **2011**, *19*, 63−69.

(2) Hasegawa, M.; Ishigami, T.; Ishii, J.; Sugiura, K.; Fujii, M. Solution-Processable Transparent Polyimides with Low Coefficients of Thermal Expansion and Self-Orientation Behavior Induced by Solution Casting. *Eur. Polym. J.* **2013**, *49*, 3657−3672.

(3) Kim, M. J.; Kim, H. G.; Kim, S. S. Composite Layer Formation on Plastic Substrates for Flexible Display by Using Functionalized Nanoclay. *Macromol. Res.* **2012**, *20*, 739−745.

(4) Wuu, D. S.; Chen, T. N.; Lay, E.; Liu, C. H.; Chang, C. H.; Wei, H. F.; Jiang, L. Y.; Lee, H. U.; Chang, Y. Y. Transparent Barrier Coatings on High Temperature Resisting Polymer Substrates for Flexible Electronic Applications. *J. Electrochem. Soc.* **2010**, *157*, C47−C51.

(5) Groner, M. D.; George, S. M.; McLean, R. S.; Carcia, P. F. Gas Diffusion Barriers on Polymers Using Al2O3 Atomic Layer Deposition. *Appl. Phys. Lett.* **2006**, *88*, 051907−3.

(6) Tsai, M. H.; Chang, C. J.; Lu, H. H.; Liao, Y. F.; Tseng, I. H. Properties of Magnetron-Sputtered Moisture Barrier Layer on Transparent Polyimide/Graphene Nanocomposite Film. *Thin Solid Films* **2013**, *544*, 324−330.

(7) Shreepathi, S.; Naik, S. M.; Vattipalli, M. R. Water Transportation Through Organic Coatings: Correlation Between Electrochemical Impedance Measurements, Gravimetry, and Water Vapor Permeability. *J. Coat. Technol. Res.* **2012**, *9*, 411−422.

(8) Park, S. H.; Lee, H. S.; Choi, J. H.; Jeong, C. M.; Sung, M. H.; Park, H. J. Improvements in Barrier Properties of Poly(lactic acid) Films Coated with Chitosan or Chitosan/Clay Nanocomposite. *J. Appl. Polym. Sci.* **2012**, *125*, E675−E680.

(9) Huang, H.-D.; Ren, P.-G.; Chen, J.; Zhang, W.-Q.; Ji, X.; Li, Z.-M. High Barrier Graphene Oxide Nanosheet/Poly(vinyl alcohol) Nanocomposite Films. *J. Membr. Sci.* **2012**, *409−410*, 156−163.

(10) Findenig, G.; Leimgruber, S.; Kargl, R.; Spirk, S.; Stana-Kleinschek, K.; Ribitsch, V. Creating Water Vapor Barrier Coatings from Hydrophilic Components. *ACS Appl. Mater. Interfaces* **2012**, *4*, 3199−3206.

(11) Tsai, M. H.; Wang, H. Y.; Lu, H. T.; Tseng, I. H.; Lu, H. H.; Huang, S. L.; Yeh, J. M. Properties of Polyimide/Al2O3 and Si3N4 Deposited Thin Films. *Thin Solid Films* **2011**, *519*, 4969−4973.

(12) Carcia, P. F.; McLean, R. S.; Groner, M. D.; Dameron, A. A.; George, S. M. Gas Diffusion Ultrabarriers on Polymer Substrates Using Al2O3 Atomic Layer Deposition and SiN Plasma-Enhanced Chemical Vapor Deposition. *J. Appl. Phys.* **2009**, *106*, 023533−6.

(13) Aulin, C.; Karabulut, E.; Tran, A.; Waišgberg, L.; Lindström, T. Transparent Nanocellulosic Multilayer Thin Films on Polylactic Acid with Tunable Gas Barrier Properties. *ACS Appl. Mater. Interfaces* **2013**, *5*, 7352−7359.

(14) Yudin, V. E.; Otaigbe, J. U.; Nazarenko, S. I.; Kim, W. D.; Korytkova, E. N. A Comparative Study on the Mechanical and Barrier Characteristics of Polyimide Nanocomposite Films Filled with Nanoparticles of Planar and Tubular Morphology. *Mech. Compos. Mater.* **2011**, *47*, 335−342.

(15) Chang, K. C.; Lu, H. I.; Lai, M. C.; Hsu, C. H.; Hsiao, Y. R.; Huang, K. Y.; Chuang, T. L.; Yeh, J. M.; Liu, W. R. Enhancement of Physical Properties of Electroactive Polyimide Nanocomposites by Addition of Graphene Nanosheets. *Polym. Int.* **2013**, *63*, 1011−1017.

(16) Tsai, M. H.; Tseng, I. H.; Liao, Y. F.; Chiang, J. C. Transparent Polyimide Nanocomposites with Improved Moisture Barrier Using Graphene. *Polym. Int.* **2013**, *62*, 1302−1309.

(17) Alexandre, B.; Langevin, D.; Médéric, P.; Aubry, T.; Couderc, H.; Nguyen, Q. T.; Saiter, A.; Marais, S. Water Barrier Properties of Polyamide 12/Montmorillonite Nanocomposite Membranes: Structure and Volume Fraction Effects. *J. Membr. Sci.* **2009**, *328*, 186−204.

(18) Suchanek, W. L.; Garces, J. M. Hydrothermal Synthesis of Novel Alpha Alumina Nano-Materials with Controlled Morphologies and High Thermal Stabilities. *CrystEngComm* **2010**, *12*, 2996−3002.

(19) Kim, J.; Im, H.; Kim, J.-m.; Kim, J. Thermal and Electrical Conductivity of Al(OH)3 Covered Graphene Oxide Nanosheet/Epoxy Composites. *J. Mater. Sci.* **2012**, *47*, 1418−1426.

(20) Tseng, I. H.; Chang, J. C.; Huang, S. L.; Tsai, M. H. Enhanced Thermal Conductivity and Dimensional Stability of Flexible Polyimide Nanocomposite Film by Addition of Functionalized Graphene Oxide. *Polym. Int.* **2013**, *62*, 827−835.

(21) Tsai, M. H.; Tseng, I. H.; Huang, S. L.; Hsieh, C. W. Enhancement of Dimensional Stability and Optical Transparency of Colorless Organo-Soluble Polyimide by Incorporation of Silica and Cosolvent. *Int. J. Polym. Mater.* **2014**, *63*, 48−56.

(22) Ganguly, A.; Sharma, S.; Papakonstantinou, P.; Hamilton, J. Probing the Thermal Deoxygenation of Graphene Oxide Using High-Resolution In Situ X-Ray-Based Spectroscopies. *J. Phys. Chem. C* **2011**, *115*, 17009−17019.
(23) Haubner, K.; Murawski, J.; Olk, P.; Eng, L. M.; Ziegler, C.; Adolphi, B.; Jaehne, E. The Route to Functional Graphene Oxide. *ChemPhysChem* **2010**, *11*, 2131−2139.
(24) Gao, Z.; Liu, J.; Xu, F.; Wu, D.; Wu, Z.; Jiang, K. One-Pot Synthesis of Graphene-Cuprous Oxide Composite with Enhanced Photocatalytic Activity. *Solid State Sci.* **2012**, *14*, 276−280.
(25) Yu, J.; Bai, H.; Wang, J.; Li, Z.; Jiao, C.; Liu, Q.; Zhang, M.; Liu, L. Synthesis of Alumina Nanosheets via Supercritical Fluid Technology with High Uranyl Adsorptive Capacity. *New J. Chem.* **2013**, *37*, 366−372.
(26) Lu, H.; Sun, H.; Mao, A.; Yang, H.; Wang, H.; Hu, X. Preparation of Plate-like Nano α-Al2O3 Using Nano-Aluminum Seeds by Wet-Chemical Methods. *Mater. Sci. Eng., A* **2005**, *406*, 19−23.
(27) Suchanek, W. L.; Garcés, J. M.; Fulvio, P. F.; Jaroniec, M. Hydrothermal Synthesis and Surface Characteristics of Novel Alpha Alumina Nanosheets with Controlled Chemical Composition. *Chem. Mater.* **2010**, *22*, 6564−6574.
(28) Casassa, S.; Demichelis, R. Relative Energy of Aluminum Hydroxides: The Role of Electron Correlation. *J. Phys. Chem. C* **2012**, *116*, 13313−13321.
(29) Potts, S. E.; Dingemans, G.; Lachaud, C.; Kessels, W. M. M. Plasma-Enhanced and Thermal Atomic Layer Deposition of Al2O3 Using Dimethylaluminum Isopropoxide, [Al(CH3)2(μ-OiPr)]2, As An Alternative Aluminum Precursor. *J. Vac. Sci. Technol., A* **2012**, 021505−12.
(30) Matsumoto, Y.; Koinuma, M.; Kim, S. Y.; Watanabe, Y.; Taniguchi, T.; Hatakeyama, K.; Tateishi, H.; Ida, S. Simple Photoreduction of Graphene Oxide Nanosheet Under Mild Conditions. *ACS Appl. Mater. Interfaces* **2010**, *2*, 3461−3466.
(31) Kim, H.; Miura, Y.; Macosko, C. W. Graphene/Polyurethane Nanocomposites for Improved Gas Barrier and Electrical Conductivity. *Chem. Mater.* **2010**, *22*, 3441−3450.
(32) Ebisawa, S.; Ishii, J.; Sato, M.; Vladimirov, L.; Hasegawa, M. Spontaneous Molecular Orientation of Polyimides Induced by Thermal Imidization (5). Effect of Ordered Structure Formation in Polyimide Precursors on CTE. *Eur. Polym. J.* **2010**, *46*, 283−297.
(33) Ovid'ko, I. A. Enhanced Mechanical Properties of Polymer-Matrix Nanocomposites Reinforced by Graphene Inclusions: A Review. *Rev. Adv. Mater. Sci.* **2013**, *34*, 19−25.